

Interactions between magnetohydrodynamic shear instabilities and convective flows in the solar interior

L. J. Silvers^{1*}, P. J. Bushby² & M. R. E. Proctor¹

¹*Department of Applied Mathematics and Theoretical Physics, University of Cambridge, Cambridge, CB3 0WA, United Kingdom*

²*School of Mathematics and Statistics, Newcastle University, Newcastle Upon Tyne, NE1 7RU, United Kingdom*

Submitted ????

ABSTRACT

Motivated by the interface model for the solar dynamo, this paper explores the complex magnetohydrodynamic interactions between convective flows and shear-driven instabilities. Initially, we consider the dynamics of a forced shear flow across a convectively-stable polytropic layer, in the presence of a vertical magnetic field. When the imposed magnetic field is weak, the dynamics are dominated by a shear flow (Kelvin-Helmholtz type) instability. For stronger fields, a magnetic buoyancy instability is preferred. If this stably stratified shear layer lies below a convectively unstable region, these two regions can interact. Once again, when the imposed field is very weak, the dynamical effects of the magnetic field are negligible and the interactions between the shear layer and the convective layer are relatively minor. However, if the magnetic field is strong enough to favour magnetic buoyancy instabilities in the shear layer, extended magnetic flux concentrations form and rise into the convective layer. These magnetic structures have a highly disruptive effect upon the convective motions in the upper layer.

Key words: convection – instabilities – (magnetohydrodynamics) MHD – Sun: interior – Sun: magnetic fields

1 INTRODUCTION

The 11 year solar magnetic cycle is driven by a hydro-magnetic dynamo. However, the exact nature of this dynamo mechanism is still not fully understood, and there are several scenarios that seek to explain the observed behaviour. The well-known “interface” dynamo model (Parker 1993), is based on the idea that the dynamo operates in a region that straddles the base of the solar convection zone and the stably stratified region that lies beneath (for some recent reviews see Ossendrijver 2003; Proctor 2006; Dormy & Soward 2007; Silvers 2008). Although this is a conceptually appealing model for the solar dynamo, the only numerical investigations of the interface dynamo have been based upon mean-field dynamo theory (see, for example, Charbonneau & MacGregor 1997; Chan, Liao, Zhang & Jones 2004; Zhang, Liao, Schubert 2004; Bushby 2006). In mean-field theory, several aspects of the dynamo model (particularly the effects of turbulent convection) are parametrised. However, the resulting coefficients are poorly determined by both theory and observations. Due to the computational costs involved, it has not yet

been possible to demonstrate the operation of the interface dynamo by carrying out three-dimensional simulations of compressible magnetohydrodynamics. Given these computational constraints, it makes sense to investigate different components of the interface dynamo in isolation.

An important feature of the region below the solar convection zone is the solar tachocline (see Spiegel & Zahn 1992; Christensen-Dalsgaard & Thompson 2007, and references therein), which takes the form of an intense radial gradient of the solar differential rotation. At the heart of the interface dynamo scenario is the idea that weak poloidal magnetic fields can be amplified by the intense shears in the tachocline, leading to the production of strong toroidal (azimuthal) magnetic fields. In the standard interface dynamo model, these poloidal magnetic fields are produced in the convection zone, and are pumped down into the tachocline by the fluid motions (Tobias *et al.* 1998, 2001). In flux transport dynamo models, these poloidal fields are transported from the surface (to the tachocline region) by a meridional circulation (see, e.g., Dikpati & Gilman 2009). Wherever the poloidal field is generated, a mechanism is needed to produce flux structures that rise through the convection zone to the surface, where they emerge to form active regions. The most natural mechanism for inducing this verti-

* E-mail: ljs53@damtp.cam.ac.uk (LJS)

cal transport is magnetic buoyancy (Parker 1955; Newcomb 1961). Strong coherent fields exert a magnetic pressure that leads to these magnetic regions becoming less dense than their surroundings. Provided that the ambient medium is not too stably stratified, instabilities can occur that would appear to allow strong fields to rise into the convection zone above. A full discussion of magnetic buoyancy and its importance in relation to tachocline dynamics can be found in Hughes (2007), while the role of the tachocline in the solar cycle is described by Tobias & Weiss (2007).

Until recently, most studies have addressed the evolution of magnetic buoyancy instabilities in a prescribed layer of magnetised fluid (see, for example, Cattaneo & Hughes 1988; Matthews, Hughes & Proctor 1995; Wissink *et al.* 2000; Fan 2001; Kersalé, Hughes & Tobias 2007). However, it is not immediately obvious that a realistic velocity shear can produce strong enough magnetic fields to become unstable to buoyancy modes, particularly in the very stably-stratified tachocline. To become buoyant the fields must exert strong Lorentz forces, which will also retard the flow and resist the field amplification. The linear evolution of magnetic buoyancy instabilities in a compressible magnetic layer, with an aligned velocity shear, was considered by Tobias & Hughes (2004). They found that magnetic buoyancy instabilities tended to be stabilised by a strong velocity shear. Recent numerical calculations have started to address the more complex problem of the non-linear evolution of shear-driven magnetic buoyancy instabilities (see, for example, Brummell, Cline & Cattaneo 2002; Cattaneo, Brummell & Cline 2006; Vasil & Brummell 2008, 2009).

Using a combination of high resolution numerical simulations and analytical calculations, Vasil & Brummell (2008, 2009) investigated the stability of a magnetic layer that is generated by the action of a strong vertical velocity shear upon an imposed uniform magnetic field. They argued that no magnetic buoyancy instability would be possible, in the stably-stratified tachocline, unless the magnitude of the velocity shear were many orders of magnitude larger than the inferred radial shear. This would have profound consequences for the hydrodynamic stability of the shear. Defining the Richardson number, Ri , to be the square of the Brunt-Väisälä frequency divided by the square of the velocity gradient, a necessary condition for hydrodynamic stability is that $Ri > 1/4$ (see, for example, Chandrasekhar 1961). In the tachocline, the Richardson number is estimated to be many orders of magnitude larger than that given by this stability bound, which implies that the shear is stable. However, if the velocity shear is strong enough that the stability condition is not satisfied, as in the calculations of Vasil & Brummell (2008, 2009), then this system will be subject to shear instabilities (of “Kelvin-Helmholtz” type). Clearly the situation becomes more complicated in the presence of an imposed magnetic field, and the subsequent evolution depends crucially (and highly non-trivially) upon the strength of this magnetic field. This is an interesting problem in its own right. Hughes & Tobias (2001) considered the linear evolution of magnetised shear instabilities, whilst the nonlinear problem has also been studied in unstratified compressible fluids (Frank, Jones, Ryu, Gaalaas 1996; Ryu, Jones, Frank 2000; Palotti, Heitsch, Zweibel, Huang 2008) as well as in

isothermal stratified layers (Brüggen & Hillebrandt 2001). The recent review article by Gilman & Cally (2007) describes global magnetohydrodynamic shear instabilities in the tachocline.

Although the hydrodynamic stability of the velocity shear was discussed by Vasil & Brummell (2008, 2009), the most important idea in their work was the suggestion that shear-driven magnetic buoyancy instabilities can only occur at very small values of the Richardson number. Since this would appear to be incompatible with the tachocline, this would have dire consequences for solar dynamo models. However, these results are not conclusive. Firstly, their calculations were all performed using a fixed value for the imposed magnetic field strength. This is clearly an important parameter, since the Lorentz force plays a crucial dynamical role. More importantly, recent calculations by Silvers *et al.* (2009) have confirmed, as already known for the onset of magnetic buoyancy without shear (Hughes 2007), that the onset of magnetic buoyancy instabilities depends upon the ratio of the magnetic to thermal diffusivities. At high Reynolds numbers, Silvers *et al.* (2009) have shown that magnetic buoyancy instabilities can be excited with a weaker (hydrodynamically-stable) shear if the thermal diffusivity is much greater than the magnetic diffusivity (something that was not the case in the original calculations of Vasil & Brummell (2008)). This is a more encouraging result from the point of view of the solar dynamo, although more work remains to be done.

Clearly, the parametric dependence of the instabilities of a forced shear flow, in the presence of a magnetic field, is still not fully understood. One of the aims of this paper is to enhance our understanding of these instabilities via a partial exploration of parameter space. In particular, we focus attention upon the effects of varying the strength of the imposed magnetic field (although some variations in other parameters are also considered). Once the evolution of this system has been studied in a single convectively-stable layer of compressible fluid, we move on to consider a more complicated “composite” model, which combines the stably-stratified shear layer with an overlying convectively-unstable region. This composite model enables us to address the interesting question, so far largely unexplored, of how buoyant magnetic flux might interact with the fluid in the lower convection zone. In order to limit the computational expense of this parametric survey, we choose a stronger velocity shear than that considered by Silvers *et al.* (2009). This enables us to drive buoyancy instabilities at lower Reynolds numbers, which means that fully resolved numerical simulations can be carried out with a coarser numerical grid. Although our chosen flow is hydrodynamically unstable, it is still much weaker than the target shear that was considered by Vasil & Brummell (2008, 2009), being mildly subsonic as opposed to highly supersonic (though still much stronger than that found within the tachocline). Although we are not exploring the rather extreme parameter regime that is directly relevant for the tachocline, our choice of parameters allows us to enhance our basic understanding of the interactions between magnetic buoyancy and convective instabilities. Future research (which will rely upon this work) will focus upon these phenomena at higher Richardson numbers.

The plan of the paper is as follows: In the next section we describe the set up of the model problem. In section 3, we

present numerical results from this model, describing the interactions between magnetic and hydrodynamic instabilities in a single stably-stratified polytropic layer. In the following section, we describe the (more complicated) problem of shear-driven instabilities in the composite model. Finally, in section 5, we conclude with a discussion of the astrophysical significance of these results.

2 THE MODEL

The model we use is similar to that of several previous studies of magnetoconvection (see, for example, Matthews, Proctor & Weiss 1995; Bushby & Houghton 2005; Lin, Silvers & Proctor 2008). We consider the evolution of a plane layer of electrically-conducting fluid, which is heated from below, in the presence of a magnetic field that is initially uniform and vertical. Accordingly, we adopt a Cartesian frame of reference such that the z -axis points vertically downwards, parallel to the constant gravitational acceleration, g . Defining d to be some characteristic length-scale (e.g. the depth of the convection zone in the composite model), this fluid occupies the region $0 \leq x, y \leq \lambda d$ and $0 \leq z \leq dz_0$. We set $z_0 = 1$ in the single layer calculations that are described in the next section (in which case d corresponds to the layer depth), whilst $z_0 = 3$ in the composite model. Varying the parameter λ enables us to change the width of the domain without altering the value of d . In contrast to most previous studies of magnetoconvection (although see the recent paper by Käpylä, Korpi & Brandenburg 2008), we investigate the evolution of this system under the influence of a forced horizontal shear flow in the x -direction.

Throughout this paper, we assume that the shear viscosity, μ , the magnetic diffusivity, η , the permeability of free space, μ_0 , and the specific heat capacities at constant pressure and density (c_P and c_V respectively) are all constant properties of the fluid. The thermal conductivity, $K(z)$, is assumed to be a function of z . Defining ρ to be the fluid density, T to be the temperature, \mathbf{u} to be the fluid velocity and \mathbf{B} to be the magnetic field, the governing equations for the evolution of this compressible fluid are given by:

$$\frac{\partial \rho}{\partial t} + \nabla \cdot (\rho \mathbf{u}) = 0 \quad (1)$$

$$\rho \left[\frac{\partial \mathbf{u}}{\partial t} + (\mathbf{u} \cdot \nabla) \mathbf{u} \right] = -\nabla P + \rho g \hat{\mathbf{z}} - \mu \nabla^2 [U_0(z) \hat{\mathbf{x}}] \quad (2)$$

$$+ \frac{1}{\mu_0} (\nabla \times \mathbf{B}) \times \mathbf{B} + \nabla \cdot (\mu \boldsymbol{\tau})$$

$$\rho c_V \left[\frac{\partial T}{\partial t} + (\mathbf{u} \cdot \nabla) T \right] = -P \nabla \cdot \mathbf{u} + \nabla \cdot [K(z) \nabla T] \quad (3)$$

$$+ \frac{\eta |\nabla \times \mathbf{B}|^2}{\mu_0} + \frac{\mu \tau^2}{2}$$

$$\frac{\partial \mathbf{B}}{\partial t} = \nabla \times [\mathbf{u} \times \mathbf{B} - \eta \nabla \times \mathbf{B}] \quad (4)$$

$$\nabla \cdot \mathbf{B} = 0, \quad (5)$$

where the pressure P satisfies the perfect gas law

$$P = R_* \rho T, \quad (6)$$

(defining R_* to be the gas constant) and the components of the viscous stress tensor $\boldsymbol{\tau}$ satisfy

$$\tau_{ij} = \frac{\partial u_i}{\partial x_j} + \frac{\partial u_j}{\partial x_i} - \frac{2}{3} \frac{\partial u_k}{\partial x_k} \delta_{ij}. \quad (7)$$

Finally the scalar quantity, $U_0(z)$, represents the horizontal shear flow. The corresponding forcing term in Equation 2 ensures that any imposed shear of this form is a solution of the horizontal component of the momentum equation (in the absence of any other motions).

The boundary conditions for these variables are consistent with those of an idealised model. All variables are assumed to satisfy periodic boundary conditions in the x and y directions. The upper and lower bounding surfaces (at $z = 0$ and $z = dz_0$ respectively), are assumed to be impermeable and stress-free, and it also assumed that the magnetic field is vertical at these boundaries. The upper boundary is held at fixed temperature, whilst the heat flux passing through the lower surface is assumed to be constant. This implies that:

$$u_z = \frac{\partial u_x}{\partial z} = \frac{\partial u_y}{\partial z} = B_x = B_y = 0, \quad T = T_0 \quad \text{at } z = 0, \quad (8)$$

$$u_z = \frac{\partial u_x}{\partial z} = \frac{\partial u_y}{\partial z} = B_x = B_y = 0, \quad \frac{\partial T}{\partial z} = C \quad \text{at } z = dz_0, \quad (9)$$

where C is a constant that will depend upon the initial conditions of the model. Note that the choice of a stress-free boundary condition for u_x implies that the imposed shear, $\partial U_0(z)/\partial z$, should also be zero at these surfaces.

These equations can be expressed in non-dimensional form, using the scalings described by Matthews, Proctor & Weiss (1995). Lengths are scaled by d , whilst the density and temperature are scaled by their initial values at the top of the layer (ρ_0 and T_0 respectively). Velocities are scaled in terms of the isothermal sound speed at the upper surface, $\sqrt{R_* T_0}$, which suggests a natural scaling for time of $d/\sqrt{R_* T_0}$. Magnetic fields are scaled in terms of the strength of the initial vertical magnetic field B_0 . Finally, we define K_0 to be the value of $K(z)$ at the upper surface. When these scalings are substituted into the governing equations, we obtain several non-dimensional parameters that are essentially identical to those described by Matthews, Proctor & Weiss (1995). These include the dimensionless thermal diffusivity, $\kappa = K_0/d\rho_0 c_P \sqrt{(R_* T_0)}$, the ratio of specific heats, $\gamma = c_P/c_V$, the Prandtl number, $\sigma = \mu c_P/K_0$, and the ratio of the magnetic to the thermal diffusivity at the top of the layer, $\zeta_0 = \eta c_P \rho_0/K_0$. Finally, $F = B_0^2/R_* T_0 \rho_0 \mu_0$ is the ratio of the squared Alfvén speed to the square of the isothermal sound speed at the top of the layer. This parameter determines the dynamical influence of any imposed magnetic field.

With appropriate choices for these non-dimensional parameters, we solve the equations numerically using a parallel hybrid finite-difference/pseudo-spectral code. In this code, time-stepping is carried out with an explicit third-order Adams-Bashforth scheme. Horizontal derivatives are evaluated in Fourier space, whilst vertical derivatives are calculated using fourth-order finite differences (upwinded derivatives being used for the advective terms). In order to carry out these simulations, grid resolutions of $128 \times 128 \times 200$ mesh points were used for the single layer cases, whilst $256 \times 256 \times 300$ mesh points were used for the composite model. Some calculations were also carried out at lower spatial resolution and comparisons of the different resolutions

| Param. | Description | Value |
|-----------|-------------------------|----------|
| σ | Prandtl Number | 0.05 |
| m | Polytropic Index | 1.6 |
| θ | Thermal Stratification | 0.5 |
| γ | Ratio of Specific Heats | 5/3 |
| κ | Thermal Diffusivity | 0.01 |
| F | Magnetic Field Strength | Variable |
| ζ_0 | Magnetic Diffusivity | 0.2 |

Table 1. Parameter values for the single layer calculations.

show that the instabilities and structures that emerge are physical and not artefacts of the discretization.

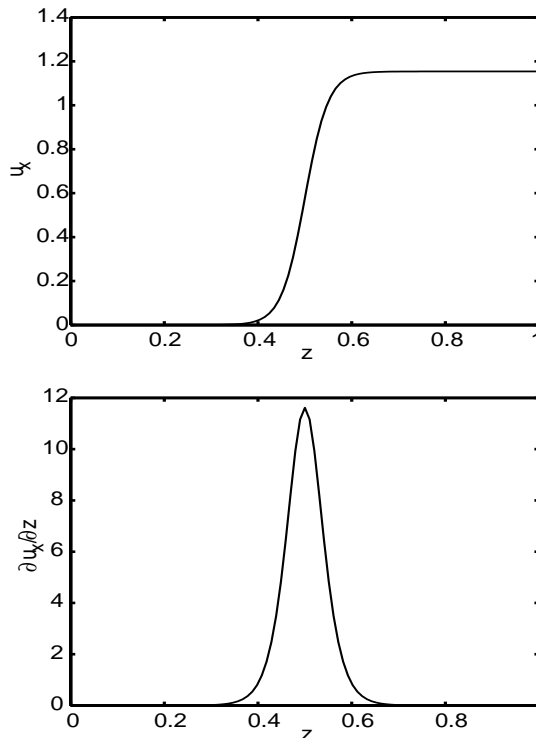
3 THE SINGLE LAYER

In this section, we consider the evolution of this system with the simplest possible initial configuration. An understanding of this system will help us to interpret the results from the next section, which deals with a much more complicated model problem. Throughout this section, we define the computational domain by setting $\lambda = 4$ and $z_0 = 1$. Recalling that all lengths are scaled in terms of d , this implies that $0 \leq x, y \leq 4$ and $0 \leq z \leq 1$.

3.1 Parameters

The behaviour of this model depends crucially upon the initial conditions that are imposed. The simplest non-trivial case to choose is that of a polytropic layer with a constant thermal conductivity, $K(z) = K_0$. In this case, the initial conditions are completely determined by two non-dimensional parameters, namely the (dimensionless) temperature difference between the upper and lower boundaries, θ , and the polytropic index, $m = gd/R_*T_0\theta$. Neglecting the effects of viscous heating, it is straightforward to show that the governing equations have the following (dimensionless) equilibrium solution: $T = (1 + \theta z)$, $\rho = (1 + \theta z)^m$, $B_z = 1$, $u_x = U_0(z)$, $u_y = u_z = B_x = B_y = 0$. Of course the effects of viscous heating will lead to a departure from this equilibrium, but we have verified (by direct calculation) that the departure is negligible over the time-scales that are considered in this paper. Therefore the above “equilibrium” solution (together with a small, random, thermal perturbation) is used as an initial condition for all the simulations that are described in this section. Note that these initial conditions imply that the lower boundary condition for temperature (see Equation 9) becomes $\partial T/\partial z = \theta$ at $z = 1$.

This system of equations has a large number of dimensionless parameters, making it impractical to conduct a complete survey of parameter space. Therefore we focus primarily upon varying the strength of the magnetic field, holding all other parameters fixed (although a small number of runs with different parameter values were also carried out). The parameter choices are summarised in Table 1. Note that this choice of θ implies that the layer is weakly stratified. Setting $m = 1.6$ and $\gamma = 5/3$ implies that stratification in the layer is mildly subadiabatic. This choice of parameters is appropriate for the

**Figure 1.** Top: u_x as a function of depth for the single layer model. Bottom: $\partial u_x/\partial z$ as a function of depth for the single layer model.

stably stratified solar tachocline (Vasil & Brummell 2008; Christensen-Dalsgaard & Thompson 2007). Note also that the parameter values that are given in Table 1 imply that the dynamical effects of the magnetic diffusivity, the viscosity and the thermal diffusivity are much more significant in this model than in the solar interior. This is because the dissipative length scales associated with the solar interior can not be resolved using any current computer. However, by setting $1 > \zeta_0 > \sigma$, we ensure that these are ordered in the same way as in the solar interior, i.e. the thermal dissipative cutoff scale is larger than the magnetic dissipative cutoff scale, which is in turn taken to be larger than the viscous scale.

Finally, we must specify a suitable initial shear flow for this system. We set

$$U_0(z) = 0.577(1 + \tanh[20(z - 0.5)]) \quad (10)$$

as shown in Figure 1(top). The hyperbolic tangent gives a smooth velocity field, varying from $u_x = 0$ at $z = 0$ up to $u_x = 1.154$ at $z = 1$. The width of the shear region is sufficiently small that the departure from a stress-free condition at the boundaries is comparable with the numerical error of the scheme. The results of Vasil & Brummell (2008) suggest that a stronger shear promotes magnetic buoyancy instabilities. We have maximised the shear velocity subject to the constraint that the horizontal flow speed never exceeds the adiabatic sound speed, whilst also ensuring that the peak mach number of the flow is identical to the peak mach number of the shear in the composite model (see the next section). Note that the fluid Reynolds number of this shear

(based upon the peak velocity and the width of the shear layer) is approximately 300, which is much smaller than in other studies (Vasil & Brummell 2008, 2009; Silvers *et al.* 2009). As discussed in the Introduction, this enables us to carry out fully resolved simulations with comparatively modest numerical grids.

3.2 Results

Having set up the model problem for a stably-stratified polytropic layer, we now investigate the effects of varying the imposed magnetic field. In order to achieve this, we carry out a series of numerical simulations for different values of the parameter, F (keeping all other parameters fixed, as shown in Table 1). In the absence of a magnetic field ($F = 0$), we find that the system is unstable to a shear flow (Kelvin-Helmholtz type) instability. Initially, we see rolls forming in the $x - z$ plane, as shown in Figure 2. This then rapidly evolves into a three-dimensional time-dependent flow. The implications of imposing a magnetic field across this computational domain depend upon the strength of the imposed magnetic field. If the initial field is weak (say $F = 1/90000$), then the effect of the field on the evolution of the instability is negligible, as the solutions are virtually indistinguishable from the hydrodynamic case. The magnetic field is simply advected with the resultant flow as a passive vector field. However, if we increase the strength of the magnetic field, we find that it starts to have a dynamical influence. Figure 3 shows the evolution of a simulation with a magnetic field strength determined by $F = 1/9000$. In this case, the magnetic field does reduce the vigour of the instability, leading to more ordered motions (particularly at early times). This behaviour is easy to explain. The shear flow instability acts so as to bend the magnetic field lines parallel to the velocity shear. A strong field tends to resist this process, thus inhibiting the instability. However even in this simulation, as in the hydrodynamic case, the instability eventually develops three-dimensional structure.

The character of the instability changes further as we increase the strength of the imposed magnetic field. Results for $F = 1/900$ are shown in Figure 4. The resulting horizontal magnetic field is now strong enough to completely suppress the shear flow instability. Rather than generating fluctuations parallel to the shear, the initial instability is a short wavelength interchange instability, with almost all variation (at least initially) in the y direction. These interchange modes are typical of a magnetic buoyancy instability (Newcomb 1961; Hughes 1985). During these early stages, the developing structures are similar to those found in two-dimensional calculations of the break up of a magnetic layer in the absence of a shear (Cattaneo & Hughes 1988). At later times some longer wavelength variation in the x direction does appear – this three-dimensional evolution is similar to that found by Wissink *et al.* (2000).

While the focus of this section is to explore the effects of varying the magnetic field strength, we note that there are other parameters that can be varied (subject to computational constraints). A reduction in the Prandtl number leads to a reduction in the viscous dissipation relative to the other diffusivities. This also increases the fluid Reynolds number. We carried out runs with lower values of the Prandtl number, and found that reducing this parameter by up to a fac-

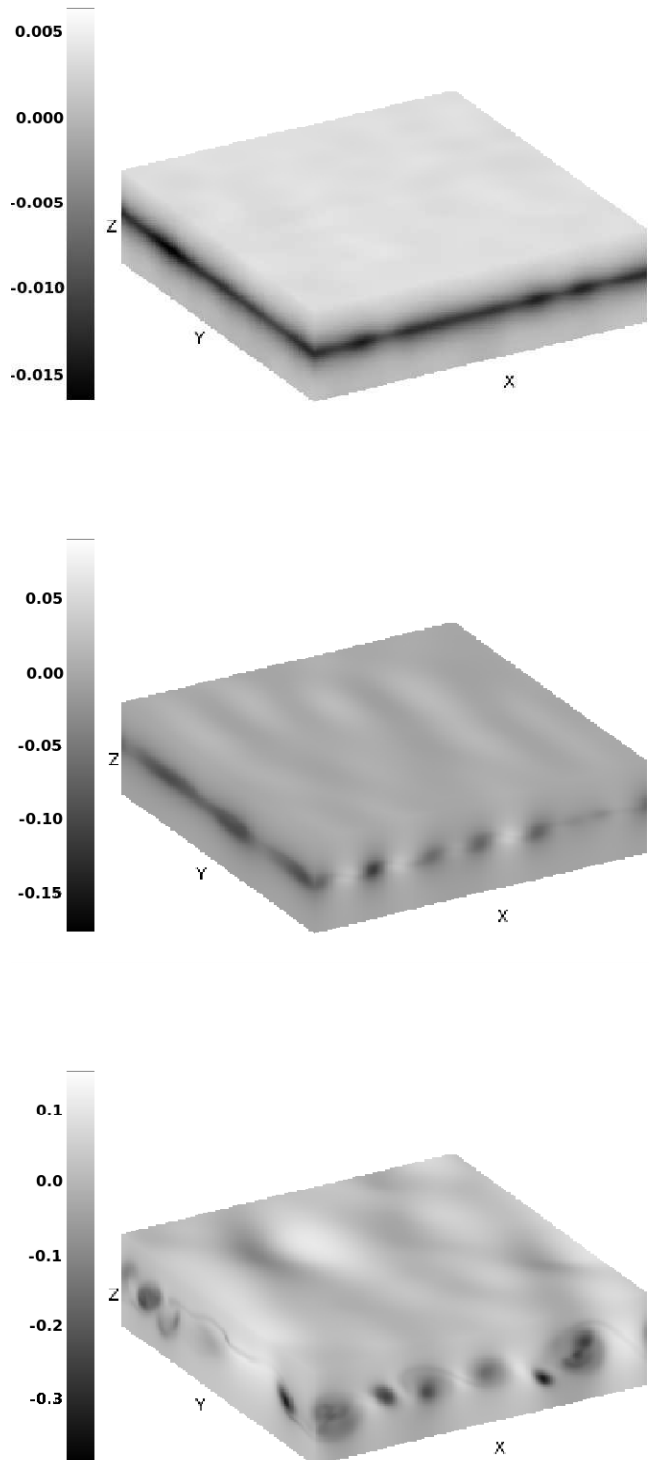


Figure 2. Density perturbation snapshot for the hydrodynamic case ($F = 0$) at times $t = 2.59$ (top), $t = 5.20$ (middle) and $t = 7.69$ (bottom)

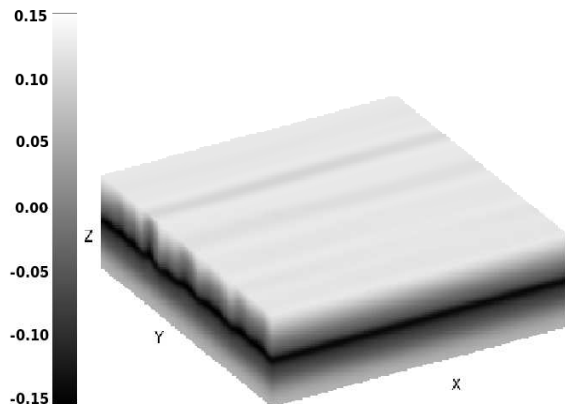
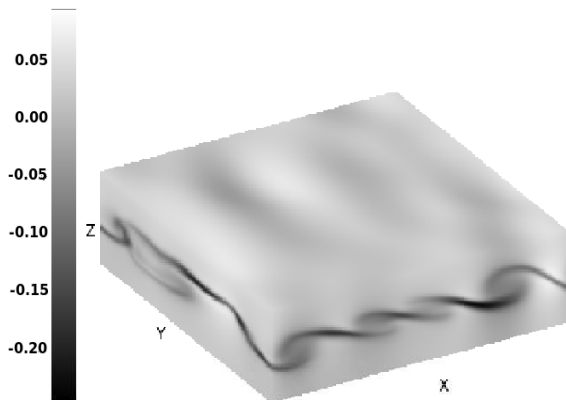
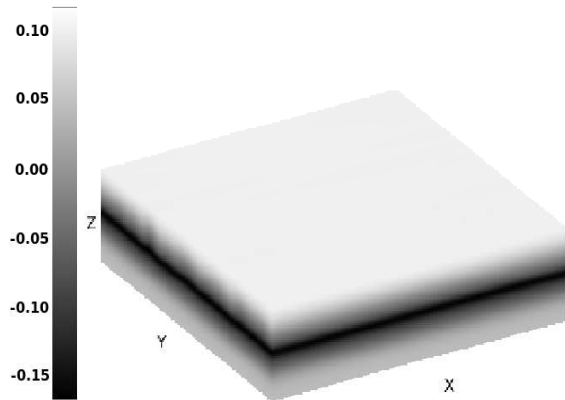
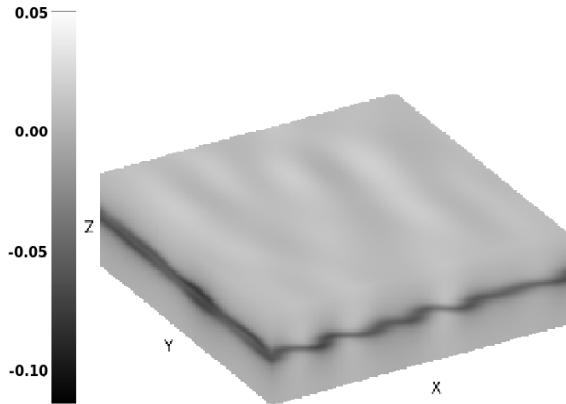


Figure 3. Density perturbation snapshot for $F=1/9000$, at $t=5.21$ and 7.78 .

Figure 4. Density perturbation snapshot for $F=1/900$, at $t=10.93$ and 13.88 .

tor of ten (going down to $\sigma \sim 0.005$) appears to have little effect upon the vigour of the instability at $F = 1/900$. This suggests that there is very little dependence upon the fluid Reynolds number in this parameter regime. The effects of varying both κ and σ have not been systematically studied here; Silvers *et al.* (2009) have shown that κ in particular can play an important role for larger values of the Richardson number, and investigation of a full range of diffusivity ratios will be the subject of future work.

4 THE COMPOSITE MODEL

In this section, we consider a more complicated model problem, consisting of a piecewise polytropic atmosphere. This is intended to be a highly idealised representation of the region straddling the base of the solar convection zone. In order to achieve this, we consider a deeper computational domain, corresponding to $z_0 = 3$. We also choose a wider computational domain, by setting $\lambda = 8$. Recalling the definitions of

these parameters, this implies that the computational domain is defined by $0 \leq x, y \leq 8$ and $0 \leq z \leq 3$.

4.1 Parameters

Other than the dimensions of the computational domain, the main difference between these calculations and those of the preceding section is that the polytropic index of the domain is now a function of depth. We split up the domain into three layers of unit depth. In the top layer ($0 \leq z \leq 1$), we choose a polytropic index of $m_0 = 1$, which implies that this region is convectively unstable. Like the single layer from the previous section, the middle region ($1 \leq z \leq 2$) is convectively stable with $m_1 = 1.6$. The lower layer ($2 \leq z \leq 3$) is also convectively stable but with a much larger polytropic index, $m_2 = 4$. The primary purpose of the lower layer is to lessen the impact of the rigid lower boundary. Any descending convective plumes that reach $z = 2$ can simply pass into the lower region without “splashing” back and interfering with the other dynamics in the system. In order to achieve

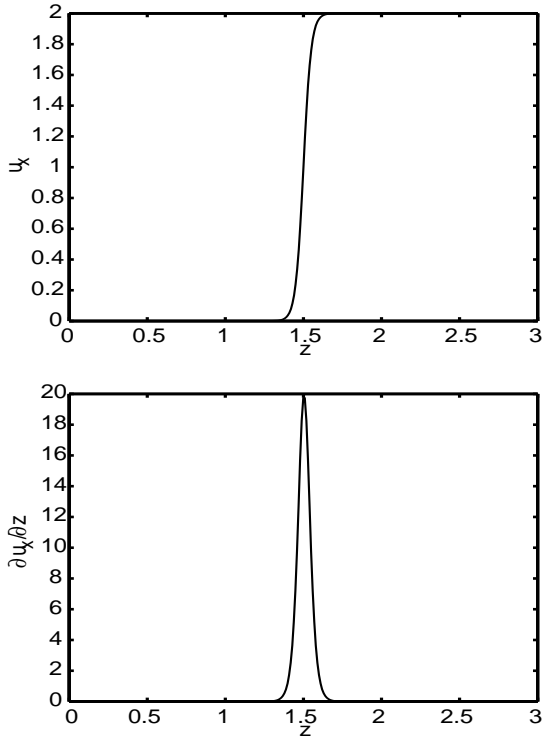


Figure 5. Top: u_x as a function of depth for the composite layer model. Bottom: $\partial u_x/\partial z$ as a function of depth for the composite layer model.

the required piecewise-polytropic structure, we choose the following depth-dependent thermal conductivity profile:

$$\begin{aligned}
 K(z) = & \frac{K_0}{2} \left[1 - \tanh\left(\frac{z-1}{0.02}\right) \right] \\
 & + \frac{K_0(m_2+1)}{2(m_0+1)} \left[1 + \tanh\left(\frac{z-2}{0.02}\right) \right] \\
 & + \frac{K_0(m_1+1)}{2(m_0+1)} \left[1 - \tanh\left(\frac{z-2}{0.02}\right) \tanh\left(\frac{z-1}{0.02}\right) \right],
 \end{aligned} \quad (11)$$

where $K_0 = K(0)$ (as before). The tanh profiles ensure that the conductivity varies smoothly between each region.

In this composite model, our aim is to investigate the effects that any shear instabilities in the mid-layer have upon an established pattern of convection. Therefore, we only introduce the shear once the convection in the upper layer has become fully developed. This is achieved by integrating the equations without any horizontal forcing until $t \approx 40$. The shear is then introduced at this point, along with the corresponding forcing term in Equation 2. Once it has been introduced, the shear has the same structure as that in the single layer model but is now centred at the mid-plane of the middle region (at $z = 1.5$). Thus the imposed shear now has the form:

$$U_0(z) = 1 + \tanh[20(z - 1.5)], \quad (12)$$

as shown in figure 5. Note that the amplitude of the shear is chosen so that the local Mach number of the flow is the same as for the single-layer case.

In the absence of any imposed shear at $t = 0$, the ini-

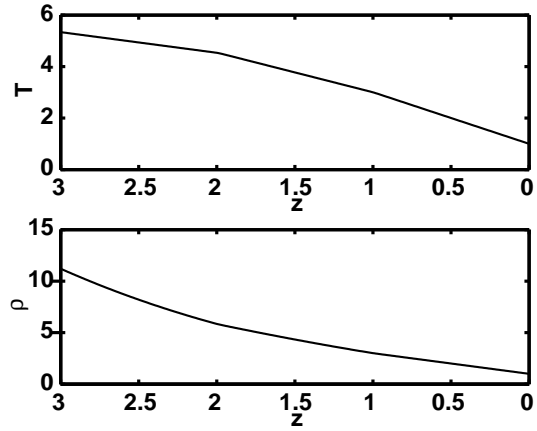


Figure 6. The initial temperature and density profiles for the composite model.

| Param. | Description | Value |
|-----------------|-------------------------|---------------|
| σ | Prandtl Number | 0.05 |
| m_0, m_1, m_2 | Polytropic Indices | 1.0, 1.6, 4.0 |
| γ | Ratio of Specific Heats | 5/3 |
| κ | Thermal Diffusivity | 0.0385 |
| F | Magnetic Field Strength | variable |
| ζ_0 | Magnetic Diffusivity | 0.1 |

Table 2. Fixed Parameter Values

tial conditions for this model differ slightly from those in the single layer case. Here we choose a magnetohydrostatic initial condition, setting $B_z = 1$ and $u_x = u_y = u_z = B_x = B_y = 0$. The equilibrium profiles for $\rho(z)$ and $T(z)$ are found numerically, and are shown in Figure 6. Note that the choice of the thermal boundary condition at the lower surface determines the extent of the thermal stratification. Setting $\partial T/\partial z = 0.8$ at $z = 3$ ensures that the temperature increases by 50% across the middle layer, as was the case for the single layer.

The parameters for this composite model are chosen so that the conditions in the middle layer are as similar as possible to those for the single layer calculation. Note that this requires some rescaling of κ and ζ_0 . These parameters are shown in Table 2.

4.2 Results

As for the single layer calculations in the previous section, we carry out a series of numerical simulations for different values of the imposed magnetic field (as measured by F). In addition to any effects upon the hydrodynamic instabilities of the shear, increasing F also reduces the vigour of any convective motions in the upper region of the computational domain.¹ The range of F is carefully chosen so that we cover

¹ Note that estimates from linear theory suggest that a value of F of approximately 0.5 is needed in order to completely suppress convective flows in the upper layer. Therefore, we are not near the convective stability boundary. If we were to increase F fur-

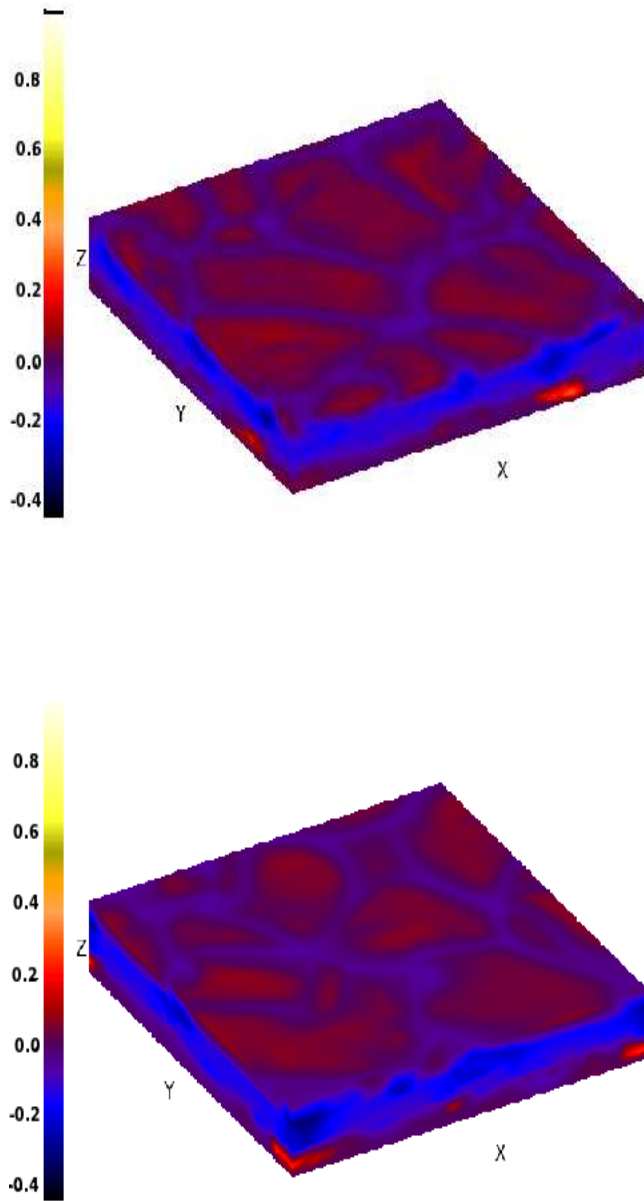


Figure 7. Three-dimensional plots of the $F = 0.0001$ case in the absence of any velocity shear. Top: The temperature perturbation on the side of the computational domain and close to the upper surface at $t \approx 40$. Bottom: The same plot at $t \approx 51$.

the same values for the mid-layer plasma beta (the ratio of the gas pressure to the magnetic pressure) that were covered in the single-layer case.

Initially, we set $F = 0.0001$, which corresponds to a

ther, we would expect to see a transition to an oscillatory mode of convection before we reach the regime in which convection is completely inhibited.

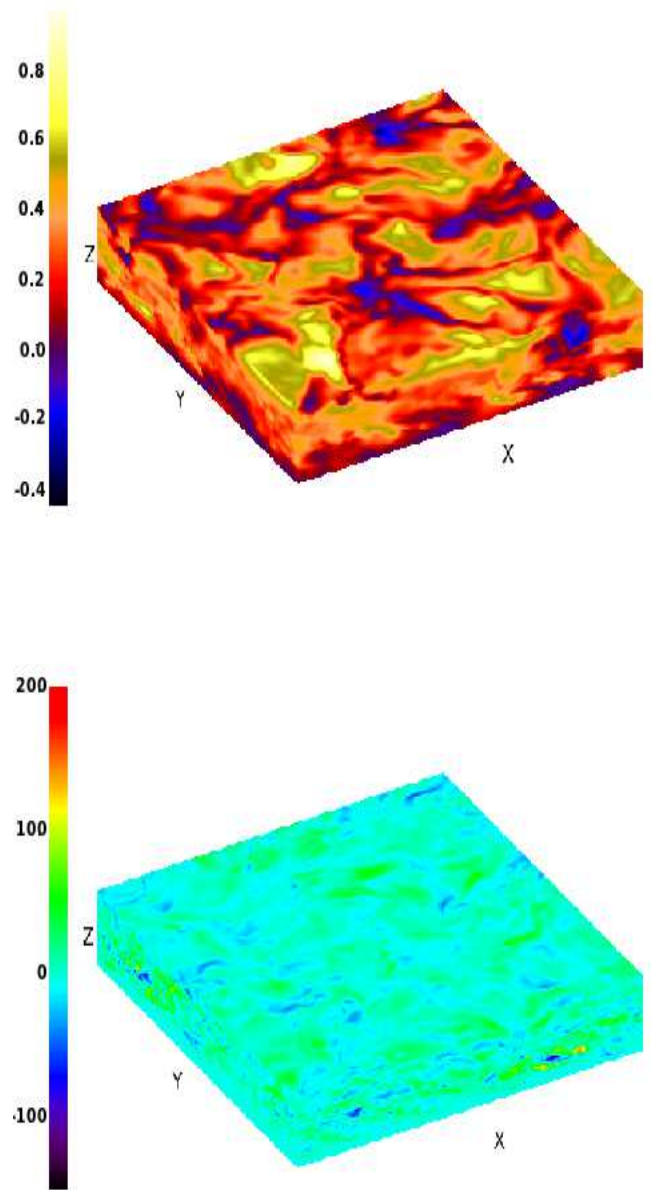


Figure 8. Three-dimensional plots of the $F = 0.0001$ case at $t \approx 51$, after the shear was introduced at $t \approx 40$. Top: The temperature perturbation on the side of the computational domain and close to the upper surface. Bottom: The horizontal magnetic field on the same surfaces. Note that in this figure, B_x is normalised with respect to the imposed field, $\propto \sqrt{F}$.

weak imposed magnetic field. Given the relative complexity of this system, we first explore the dynamics that occur in the absence of any velocity shear. This case is illustrated in Figure 7, which shows the resulting pattern of convection at $t \approx 40$ (top) and $t \approx 51$ (bottom). In the convectively unstable upper layer there is a time-dependent cellular convective pattern consisting of warm, broad upflows (which

correspond to the brighter regions in figure 7) surrounded by a network of narrower (darker) downflows. There is some modest convective overshooting into the middle layer. Figure 8 also shows a snapshot of this system at ($t \approx 51$) but, in this case, the shear is introduced at $t \approx 40$. As was found in the single-layer case, the shear is subject to a Kelvin-Helmholtz type shear instability. This rapidly develops three-dimensional structure, producing perturbations that spread throughout the stably-stratified domain, penetrating into the convective layer. Comparing Figure 7 and 8 we see that there is little evidence of anisotropy in the convecting region. However we note that there is a significant influence on the convective transport of heat in the top part of the box, which is apparently due to the influence of the shear instability on heat transport in the middle layer.

As the field strength is increased from this (effectively) kinematic level, the solutions follow a similar trend to the single-layer case. When $F = 0.001$, the dynamics in the mid-layer are similar in form to those shown in Figure 3 (although the overshooting convection from the upper layer adds some additional complexity to the resulting flows). Therefore, the dominant instability is still of Kelvin-Helmholtz type rather than a magnetic buoyancy instability, although magnetic effects are starting to play a dynamical role. Interestingly, as the shear-driven motions from the stable layer interact with the convective layer, there appears to be a slight tendency for an elongation of the convective cells in the direction of the shear. This is a phenomenon that becomes more pronounced as F is increased.

Increasing the field strength still further, so that $F = 0.01$, we find that the dynamics change dramatically. This case is illustrated in Figures 9 and 10. The imposed vertical magnetic field is now strong enough to reduce the vigour of the convection, though it has little effect on the horizontal scales of motion. Once the shear is introduced, the evolution is dominated by the shear-driven instabilities at the mid-layer. As in the single layer case, a transition has occurred so that the dominant instability is now magnetic buoyancy. Initially, this buoyancy instability takes the form of a two-dimensional (interchange) mode, although it soon develops three-dimensional structure, forming arching regions of magnetic flux that rise up through the convective upper layer of the domain. As these magnetic regions reach the upper layers, we see some concentration of the vertical magnetic flux, which forms localised concentrations near the horizontal boundaries of these rising features. The subsequent motion is now strongly anisotropic, producing convective cells that are predominantly aligned with the direction of the shear and the buoyant horizontal magnetic flux concentrations. We note that the introduction of a shear flow at $t \approx 40$ again leads to larger temperature deviations in the convectively-unstable region at later times (compared with the unsheared case). However this effect seems to become less pronounced as the field strength is increased. We attribute this phenomenon to the fact that there is less mixing in the stronger field regime, where there are larger structures present than in the weaker field cases.

The phenomena discussed above can be related to previous work on isolated buoyant flux tubes rising through the convection zone (see, for example, Jouve & Brun 2007). Even though the tubes are isolated they have been shown to interact strongly with the convective flow. The present prob-

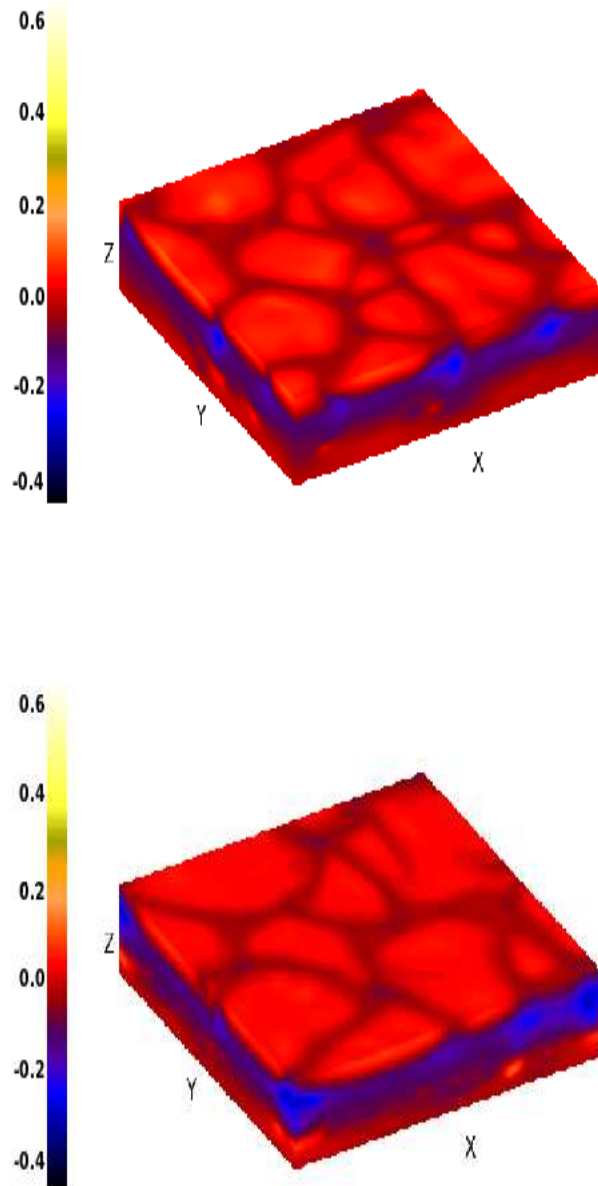


Figure 9. Three-dimensional plots of the $F = 0.01$ case in the absence of any velocity shear. Top: The temperature perturbation on the side of the computational domain and close to the upper surface at $t \approx 40$. Bottom: The same plot at $t \approx 51$.

lem is different in that the magnetic field is initially vertical. However, the shear creates a strong horizontal magnetic field and so the ultimate configuration is not dissimilar.

5 CONCLUSIONS

In this paper, we have presented some novel calculations to investigate the ways in which an imposed magnetic field in-

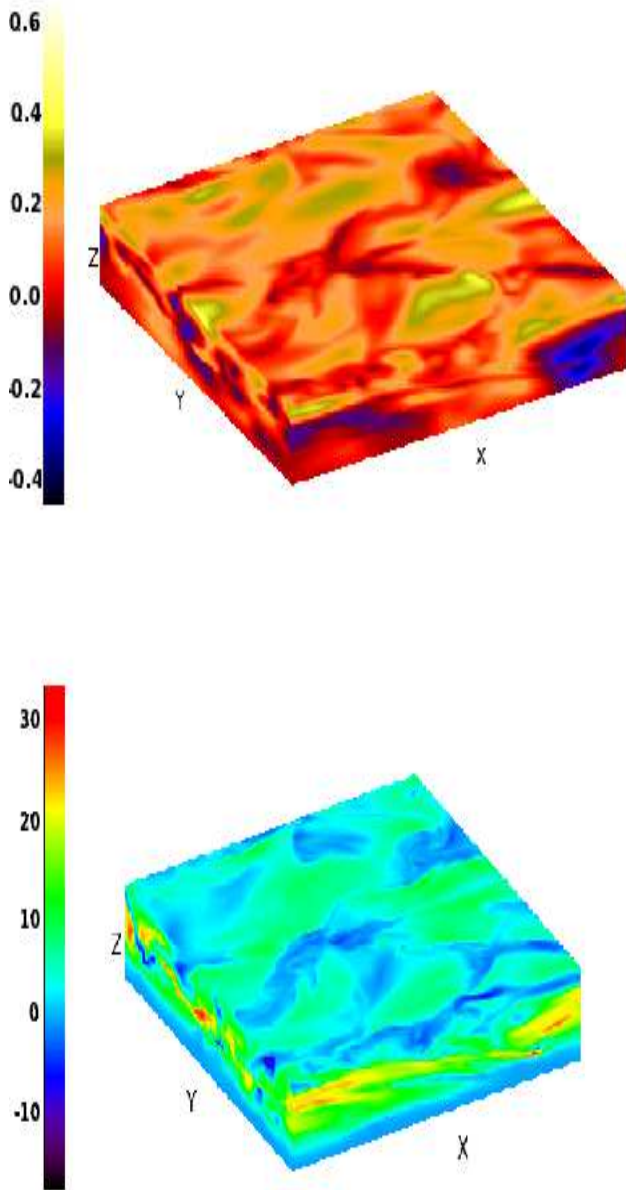


Figure 10. Three-dimensional plots of the $F = 0.01$ case at $t \approx 51$, after the shear was introduced at $t \approx 40$. Top: The temperature perturbation on the side of the computational domain and close to the upper surface. Bottom: The horizontal magnetic field on the same surfaces. Note that in this figure, B_x is normalised with respect to the imposed field, $\propto \sqrt{F}$.

teracts with a shear flow in a convectively-stable layer (both with and without an overlying convective region). This investigation was motivated by conditions at the base of the convection zone, and is relevant to the interface scenario for the solar dynamo. The most important interactions between the shear layer and the convective region are due to the rising plumes that are induced by magnetic buoyancy. In

the solar context the tachocline region, where the shear is expected to reside, is very stably stratified and there are questions regarding the efficacy of magnetic buoyancy in this situation (see, for example, Vasil & Brummell 2009). Nonetheless we know that buoyancy instabilities do occur in the Sun, and so it seems worthwhile trying to understand aspects of their evolution, even though the correct parameter range might not yet have been reached. In this context, it is also worth noting that a diffusive instability, which is effective only when the thermal diffusivity is much higher than in the present paper, appears to allow for buoyancy-induced motion even when the shear is hydrodynamically stable, according to the Richardson number criterion. This mechanism been discussed for several decades (see, for example, the discussions in Gilman 1970; Hughes 2007) but has only recently been demonstrated numerically in our geometry (Silvers *et al.* 2009).

In our “strong-shear” parameter regime, there is an instability of the shear (of Kelvin-Helmholtz type) even when there is no magnetic field. This instability leads initially to perturbations that are primarily in the $x - z$ plane. This instability subsequently develops structure in the y direction. We find that, for a sufficiently strong magnetic field, the hydrodynamic instability is suppressed, leading to a magnetic buoyancy instability with strong variations in the y direction, i.e. the direction perpendicular to both gravity and the shear flow. For calculations of the “composite model”, the most important interactions between the shear layer and the convective region are due to the rising plumes that are induced by this magnetic buoyancy instability. This instability generates strong horizontal concentrations of magnetic flux that then rise through the convective layer. For the strongest fields surveyed, the dynamical effects of these flux concentrations are so significant that they destroy the convective pattern that would normally exist in the absence of a magnetic field. As with isolated flux tubes (see, for example, Jouve & Brun 2007) they effectively push the convective motion aside. It is important to note that even our strongest imposed field has a relatively weak effect upon the horizontal scales of convection that occur in the absence of shear.

Our results are encouraging in that they show that there exists the possibility of inducing strong buoyant magnetic flux structures through the action of horizontal shear. However they are preliminary calculations in the sense that they do not allow the buoyant flux structures to rise very far. We intend to perform further calculations, with a much deeper convective zone, so as to understand the later evolution of the rising flux structures. We also note that there is a swift transition as we vary our parameters between essentially passive structures and ones that strongly disrupt the convection layer. We intend to carry out a more extensive investigation of intermediate parameter ranges in which the role of downward pumping is important in counteracting the buoyancy effects (Tobias *et al.* 2001). Finally, we intend to explore the interactions between shear-driven buoyancy instabilities and convective flows at higher Richardson numbers (with a hydrodynamically stable shear). This will be a challenging problem to tackle numerically (requiring high numerical resolution), but results from these preliminary calculations constitute a firm foundation for future work.

ACKNOWLEDGEMENTS

The authors thank Nic Brummell, Nigel Weiss and Geoff Vasil for stimulating discussions.

The numerical calculations were carried out on the UKMHD cluster based in St Andrews, which is partially funded by STFC. This research is supported via a rolling grant from STFC that is held at DAMTP, University of Cambridge. PJB and LJS also wish to acknowledge support from the KITP, Santa Barbara and travel grants from the RAS to facilitate attendance at a workshop where some of the work was done.

REFERENCES

- Bushby P. J., Houghton S. M., 2005, MNRAS, 362, 313.
 Bushby P. J., 2006, MNRAS, 371, 772.
 Brüggén, M., Hillebrandt, W., 2001, MNRAS, 323, 56.
 Brummell, N., Cline, K., Cattaneo, F., 2002, MNRAS, 329, L73.
 Cattaneo F., Hughes D. W., 1988, JFM, 196, 323.
 Cattaneo F., Hughes D. W., 2006, JFM, 553, 401.
 Cattaneo F., Brummell N., Cline K. S., 2006, MNRAS, 365, 727.
 Chan, K. H., Liao, X., Zhang, K., Jones, C. A., 2004, A&A, 423, 37.
 Chandrasekhar, S., 1961, Hydrodynamic and Hydromagnetic Stability, Pub. Dover.
 Charbonneau, P. & MacGregor, K. B., 1997, ApJ, 486, 502.
 Christensen-Dalsgaard, J. & Thompson, M. J., 2007, Ch. 3 in The Solar Tachocline, CUP.
 Dikpati, M. & Gilman, P.A., 2009, Space Science Reviews, DOI 10.1007/s11214-008-9484-3.
 Dormy E. Soward A. (eds), 2007, Mathematical Aspects of Natural Dynamos, CRC Press.
 Frank, A., Jones, T. W., Ryu, D., Gaalaas, J. B., 1996, ApJ, 460, 777.
 Fan Y., 2001, ApJ, 546, 509.
 Hughes, D. W., 1985, GAFD, 32, 273.
 Hughes, D. W., Tobias, S. M., 2001, Proc. Roy. Soc. A., 457, 1365.
 Hughes, D. W., 2007, The Solar Tachocline, pp 275–298 (CUP).
 Käpylä P. J., Korpi M. J., Brandenburg, A., 2008, A&A, accepted.
 Gilman, P.A., 1970, ApJ, 162, 1019.
 Gilman, P.A. & Cally, P.S., 2007, The Solar Tachocline, pp 243–274 (CUP).
 Kersalé E., Hughes D. W., Tobias S. M., 2007, ApJ, 663, L113
 Jouve, L., & Brun, A. S., AN, 2007, 328, 10, 1104.
 Lin, M.-K. Silvers, L. J. & Proctor, M. R. E., 2008, Phys. Lett. A, 373, 1, 69.
 Matthews P. C., Hughes D. W., Proctor M. R. E., 1995, ApJ, 448, 938.
 Matthews P. C., Proctor M. R. E. Weiss N. O., JFM, 305, 281.
 Moffatt H. K., 1978, Magnetic field generation in electrically-conducting fluids, CUP: Cambridge.
 Newcomb, W. A., 1961, Phys. Fluids, 4 391.
 Ossendrijver M. 2003, Astron. Astrophys. Rev., 11, 287.
 Palotti, M. L., Heitsch, F., Zweibel, E. G., Huang, Y.-M., 2008, ApJ, 678, 234.
 Parker E. N., 1955, ApJ, 121, 491.
 Parker E. N. 1993, ApJ, 408, 707.
 Proctor, M.R.E. 2006, EAS Pubs Series, 21, 241-273.
 Ryu, D., Jones, T. W., Frank, A. 2000, ApJ, 545, 475.
 Silvers L. J, 2008, Phil. Roy. Trans. Soc. A., 366, 4453.
 Silvers, L.J., Vasil, G.M., Brummell, N.C. & Proctor, M.R.E., 2009, ApJL, submitted .
 Spiegel E. A., Zahn J.-P., 1992, Astron. Astrophys., 265, 106.
 Tobias S. M., Brummell N. H., Clune T. L. Toomre, J., 1998, ApJL, 502, 177.
 Tobias S. M., Brummell N. H., Clune T. L., Toomre J., 2001, ApJL, 549, 2, 1183.
 Tobias S. M., Hughes, D. W., 2004, ApJ, 603, 785.
 Tobias, S.M. & Weiss, N.O., 2007, The Solar Tachocline, pp 319–350 (CUP).
 Vasil G. M., Brummell N. H., 2008, ApJ, 686, 709.
 Vasil G. M., Brummell N. H., ApJ, 690, 783.
 Wissink, J. G., Matthews, P. C., Hughes, D. W., Proctor, M. R. E., 2000, ApJ , 536, 2, 982-997.
 Zhang, K., Liao, X. Schubert, G., 2004, ApJ, 602, 468.